Northumbria Research Link

JADVE

Journal of Advances in Vehicle Engineering 2(1) (2016) 1-20
www.jadve.com

Static Tire Properties Analysis and Static Parameters Derivation to Characterising Tire Model Using Experimental and Numerical Solutions

Chongfeng Wei[a]*, Xiaoguang Yang[b]

[a] *School of Mechanical Engineering, University of Birmingham, Birmingham B15 2TT, UK*
[b] *R&D Center at South China Tire & Rubber Co., Ltd*

(Manuscript Received: 12 December 2015; Revised: 10 February 2016; Accepted: 10 March, 2016)

Abstract

Tire-ground interaction plays substantial role in determining vehicle kinetics and kinematics yet a clear understanding of such an interaction outputs is complex process. The present study aims at static analysis of tire parameters using both experimental and numerical based finite element method (FEM) solutions. To this end, tire cross section shape with different inflation pressures, vertical stiffness together with the footprint were measured using controlled apparatus and then are compared with the simulation results in order that the accuracy of the FE tire model in static condition can be validated. The 3D tire model was obtained by revolving the 2D axisymmetric tire model, and static stiffness and footprint were predicted using the 3D model. Inflation pressure analysis was presented by comparing the tire cross-section shape variation at different inflation pressures. The conclusions will serve future investigations as a concise knowledge source to develop improved tire models.

Keywords: Contact area; FEM; Footprint; Tire

1. Introduction

The industry of automotive engineering has ever-increasingly paid attention to the domain of vehicle dynamics that is closely engaged with the vehicle performance and ride comfort that are characterized as the most prominent factors in the competing market for customers. The tire analysis has been a dynamic field of studying interest in this regard. Wheels are the unique connections between the road and vehicle body and subject to all of forces and moments applied to the vehicle. Furthermore, wheels are responsible for most of kinetics of motion such as braking/acceleration, steering, traction, stability and handling. Also as an important component of vehicle suspension system, tire and its mechanical properties are deterministic on the ride comfort performance. Prior to any deep understanding of vehicle motion particularly travelling on irregular terrains and off-road paths, it is necessary to determine the tire-ground interaction. To this end, one should make a comprehensive study on tire characteristics and parameters that affect the motion of the vehicle performance. Given that based on the development of new vehicle concepts and the improvements of dynamic behavior of vehicle components, vehicle simulation with appropriate tire models is gaining more and more importance. It is noteworthy that tire models should be comprehensive to include the non-linear deformation and enveloping characteristics which occur when traversing large road obstacles.

Tire models particularly those of flexible ring based tires (FTire) are considered as complex in-plane and out-of-plane dynamic and non-linear virtual tire model being valid for both higher-frequency and short-wavelength tire model. It is also reliable model in the automotive industry for vehicle durability, road load, and ride comfort predictions [1]. However, even in order to run such a reliable closed-form model, there is a need to determine the tire contact patch characteristics and thus any model is dependent on a set of experimental data to be developed. Due to the stochastic and nonlinear characteristic of tire behavior, however, it has always been a challenging task to accurately determine the tire parameters such as contact patch area, footprint shape, longitudinal/lateral stiffness, etc.

There are studies documented in literature dealing with determining tire properties for different operating conditions. Analytical tire models have been developed to describe the complex performance of the pneumatic tire and its interaction with the road surface. These models are developed based on the physical characteristics and behavior of tires.

The analytic models were laid foundation many years ago. An elastic shell was used to represent a pneumatic tire, and the equations of tire motions were established using energy methods. The effect of elastic property and inflation pressure of the cylindrical shell were considered for establishment of the equations of motion [2]. The circular cylindrical shell was also used in another investigation [3] to represent a truck tire model. The objective of theoretically modelling truck tires, in this case, was to describe the sound radiation due to the vibration of in-service truck tire surfaces.

Three kinds of analytical tire models were investigated including point contact tire model, fixed footprint tire model and

*Corresponding author. C. Wei (*)
Department School of Mechanical Engineering, University of Birmingham, Birmingham B15 2TT, UK
e-mail: weichongfeng@gmail.com

adaptive footprint tire model, from which they found the point contact tire model was only suitable for calculation of vertical response for the tire of low natural frequency, while the footprint tire model was difficult to be adopted in a terrain-vehicle system for dynamic simulation because of its nonlinear and complex properties although they had satisfactory validations of the vertical responses [4]. As one of the basic properties, tire static stiffness has been investigated by many researchers. In the research of Kao about tire radial stiffness, the tire model was defined by a two-spring-and-two mass system, and the tire stiffness was independent of the acceleration of the tire. In their model, the radial stiffness is determined by the tire patch enveloping stiffness and the sidewall stiffness, which was determined by the measurement of the length of the contact patch [5-6].

Shim and Margolis [7] presented a new analytical tire model for simulation of tire braking and cornering at normal driving conditions. As there is a linear region for the low slip angle of the tire, the analytical model was developed for prediction of pure braking, pure cornering and combined braking and cornering properties in this region. The longitudinal forces and cornering forces of the tire were derived as a function of tire/road friction coefficient, slip angles, and normal load.

Empirical models were often derived based on the experimental data. Some purely empirical tire models have been developed to get over the inaccuracy of simple analytical tire model. Guan *et al.* [8-9] established a tire model for cornering properties by extracting experimental modal parameters under different inflation pressures, vertical loads and friction coefficients. Experimental modal parameters were extracted from longitudinal and vertical responses under excitations. The lateral force distribution in the contact patch and the deformation of carcass and tread were predicted based on the empirical tire model.

Guo and Ren [10] developed a unified semi-empirical tire model, the input parameters of which can be identified by pure longitudinal slip and side slip tests of the rolling tire, from which the lateral force, longitudinal force as well as self-aligning moment can be predicted.

Finite element method (FEM) has also shown great applicability and promising performance in analysis of vehicle components and performance. Document is abundant with those of researches dealing with numerical analysis of vehicle performance, tire characteristics and tire-ground interaction parameters [11-12]. Prediction of automobile tire cornering force characteristics by finite element modeling and analysis was conducted in an investigation. A detailed finite element model of a radial automobile tire was constructed for the prediction of cornering force characteristics during the design stage. The nonlinear stress–strain relationship of rubber as well as a linear elastic approximation, reinforcement, large displacements, and frictional ground contact were modeled [13]. The fundamental formulations on modeling soil compaction and tire mobility issues were covered while a Drucker–Prager/Cap model was implemented in ABAQUS to model the soil compaction and a user subroutine for finite strain hyperelasticity model was developed to model nearly incompressible rubber material for tire [14].

Tire basic static properties (behaviour under inflation pressure, static stiffness, and footprint) are very important tire characteristics. The natural frequencies of the vertical vibration of tires are related to the tires' vertical stiffness. Inflation pressure analysis can provide important information for the tire designers and researchers about the shape variation of the tire cross-section under different inflation pressures. For the tire traversing obstacles, the rolling tire is excited by road obstacles through vertical stiffness of the tire. Static vertical stiffness validation was carried out for different inflation pressures. Longitudinal stiffness is also an important parameter for the longitudinal characteristics of the tire, such as braking analysis and rolling resistance generated on the uneven road, which will be described in the further chapters. As the only connection between the road and the tire, the contact footprint is another important characteristic in the static property of the tire, in which the shape and size together with pressure distribution of the contact footprint are important in ride quality and handling properties of a vehicle.

The aim of present work is to determine the static tire properties and developing numerical based Finite Element Method (FEM) to validate the results. To this end, tire cross section shape with different inflation pressures, vertical stiffness together with the footprint were measured using controlled apparatus and then are compared with the simulation results in order that the accuracy of the FE tire model in static condition can be validated.

2. Materials and Method

2.1. Inflation Property Analysis

The application of inflation pressure is perhaps the simplest and most fundamental method, and the inflation analysis can be conducted conveniently using Finite Element code. Tire inflation modelling is the first step of tire static properties simulations, and the inflation pressure analysis can be carried out using two dimensional axi-symmetric tire models.

2.1.1. Inflation Pressure Simulation

As a commercial Finite Element code, ABAQUS™ is capable of modelling deformation of rubber material under different values of inflation pressure. In order to carry out inflation analysis, boundary conditions were defined in the 2D axisymmetric model. In this study, the wheel center was fixed by constraining four degrees of freedom of the tire cross-section (two translational degrees and two rotational degrees). In order to constrain the bead nodes of the tire model, a rigid body between rim node and the tire-rim assembly nodes was defined using the tie function in ABAQUS. From this way, it is more convenient to apply boundary conditions on the rim reference node to stabilize the tire-rim interface. The inflation

of the tire is modelled by application of a uniform internal pressure, which is shown in Fig. 1. In order to investigate the effect of inflation pressure variation, five different inflation pressures were applied on the tire model for simulation, which were 40kPa, 80kPa, 120kPa, 160kPa and 200kPa. About 16 nodes at half of the cross-section were selected to describe the inflation behavior at different operating conditions by calculating the displacement variation of these points. Because of the axisymmetric property of the tire, half of the cross-section displacement is sufficient to describe inflation behavior of the whole tire model. The coordinate data of these nodes at different values of inflation pressure is shown in Fig. 2.

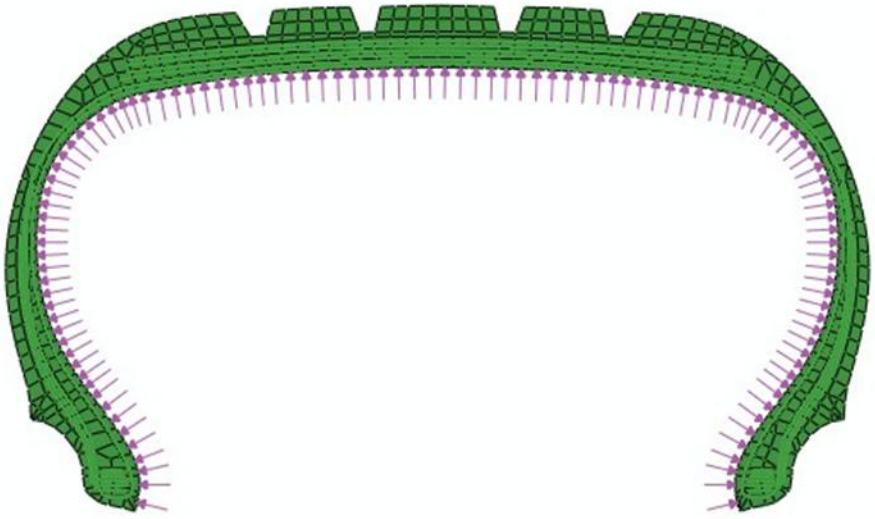

Figure 1. Inflation pressure on the 2D tire model

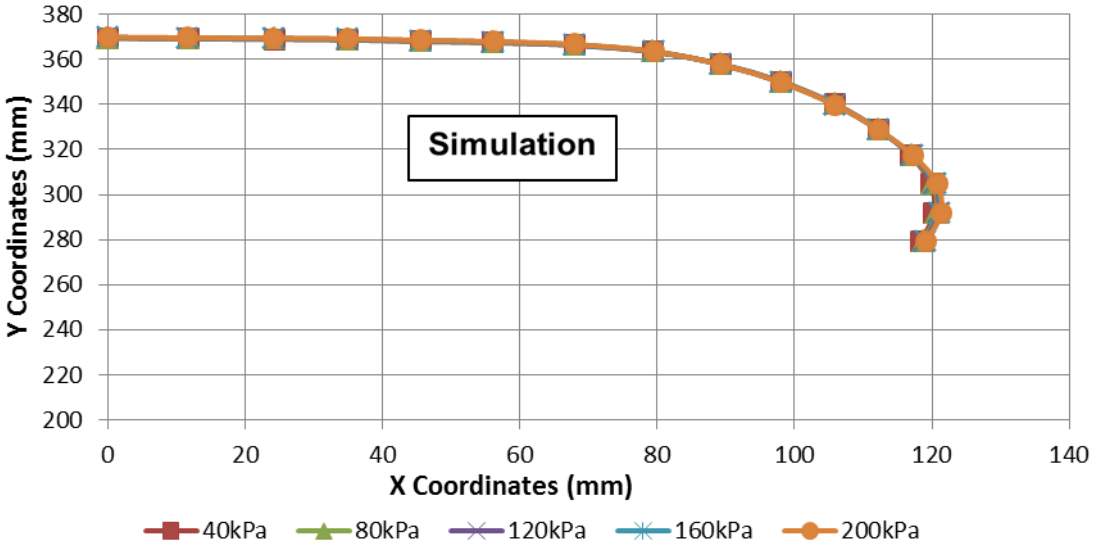

Figure 2. Pressure/Displacement profile at different inflation conditions in simulation

2.2.2. Experimental measurement of inflated tire

Properties of inflation pressure were investigated in terms of the relationship between inflation pressure and tire deformation, which could be measured at the nodes' positions of the tire cross-section. The displacement of any prescribed node can be determined by comparing the node positions at non-inflated status and inflated status. In order to validate the nodes position variation, some points need to be marked on the profile of the tire in advance. The coordinate's data of the marked points at tire profile were obtained by using the Coordinates Measurement Machine (CMM), which is shown in Fig. 3. With a flexible touch trigger of CMM, the facility could be efficient in measurement of the tire profile geometry with different values of inflation pressure, so that the relationship between pressure and displacement can be determined.

However, because the modelling file of tire cross-section data was extracted from tire cutting, and the tire file for measurement data was from an assembled balance tire with rim, not all the corresponding nodes of the FE tire cross-section model could be located on the real tire file, which is one of the difficulties in carrying out displacement testing of the tire profile. However, enough points were marked on the tire profile, which could reflect the pressure/displacement properties with coordinate measurements at different values of inflation pressure.

The CMM has the capability to measure the coordinates of the points in three dimensions. Because the measurement was carried out at the outside surface of the tire cross-section from the bead area to the center of the tread area, only coordinates at X direction and Y direction were recorded, which is illustrated at Fig. 4. Due to the axisymmetric characteristic of the tire, half of the cross-section measurement is used to represent the inflation behavior of the whole tire profile.

Eighteen different points were marked on the outside surface of the cross-section, which was convenient for the CMM to touch and acquire the coordinates of these points. Five different operating conditions were applied on the tire in terms of different values of inflation pressure. Corresponding to the condition of Finite Element model, the same range of inflation pressures were adopted in the measurement, which were 40kPa, 80kPa, 120kPa, 160kPa and 200kPa. The results at different inflation conditions are shown in Fig. 5.

However, the Fig. 5 cannot clearly describe the difference between the original shape and inflated shape of the tire. In order to efficiently investigate the displacement variation of the tread and the sidewall when the tire was inflated, two representative nodes from the tread and sidewall of the 2D tire model were chosen to validate their displacements. The displacement of the node A (in the center of the tread area) of the tread section in Y direction and the displacement of the node B (at the outermost point in sidewall area) of the sidewall section in X direction were considered and calculated at different inflation pressure conditions (Fig. 6). Note that node A's displacement represents the tread's displacement relative to the tire center, while node B's displacement represents the width variation of the tire. The variation of the displacement of node A in Y direction under different inflation pressures is shown in Fig. 7, while Fig. 8 presents the variation of the displacement of node B in X direction with increase of inflation pressure.

It can be seen in Fig. 7 and Fig. 8 that the simulation results agree well with the measurement results for both the sidewall node and the tread node. By analyzing the variation of the displacement of the sidewall in different inflation pressure conditions, it was found that the displacement of the tread in Y direction has a nearly linear relationship with the inflation pressure. The displacement of the sidewall in X direction is increasing with the increment of the inflation pressure, but the increasing magnitude of the displacement is gradually reduced.

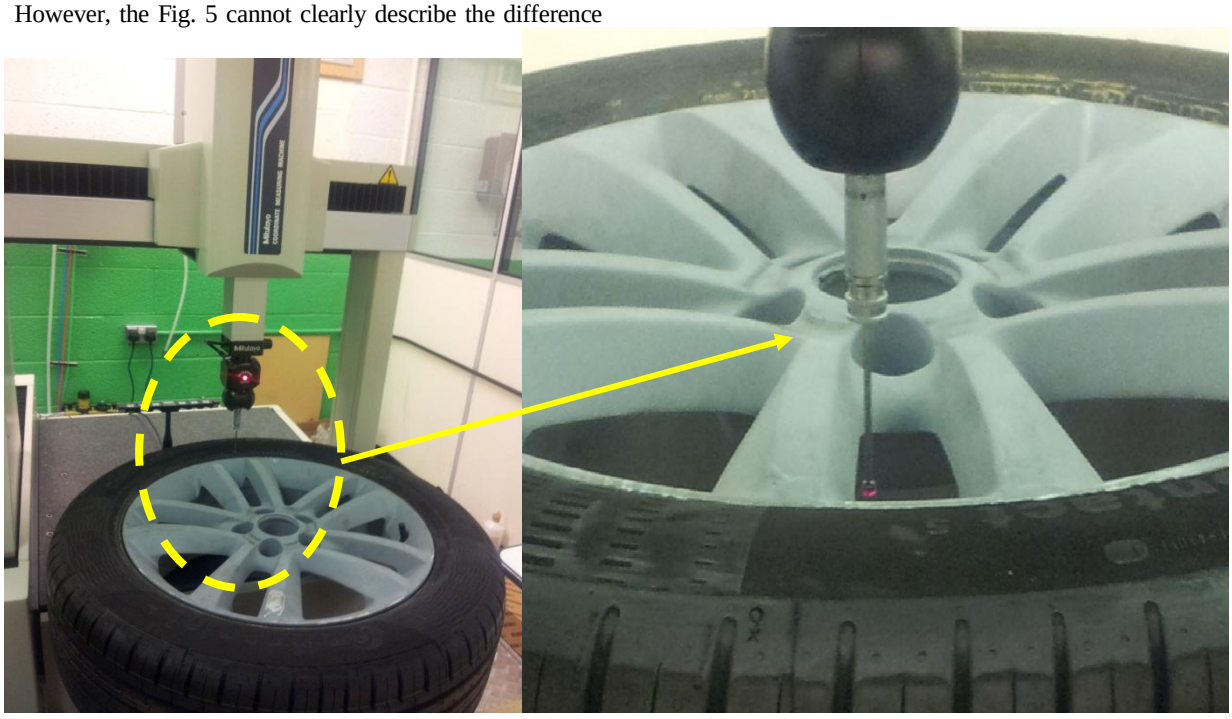

Figure 3. Coordinates Measurement Machine for tire inflation shape measurement

Figure 4. Representation of the tire lying on the testing table

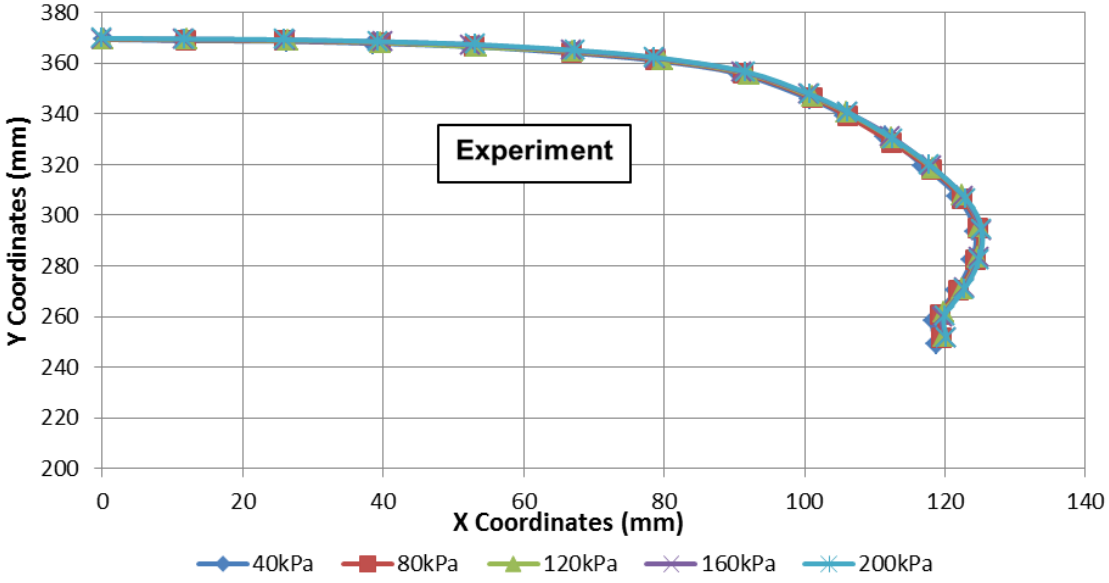

Figure 5. Pressure/Displacement profile at different inflation conditions in experiment

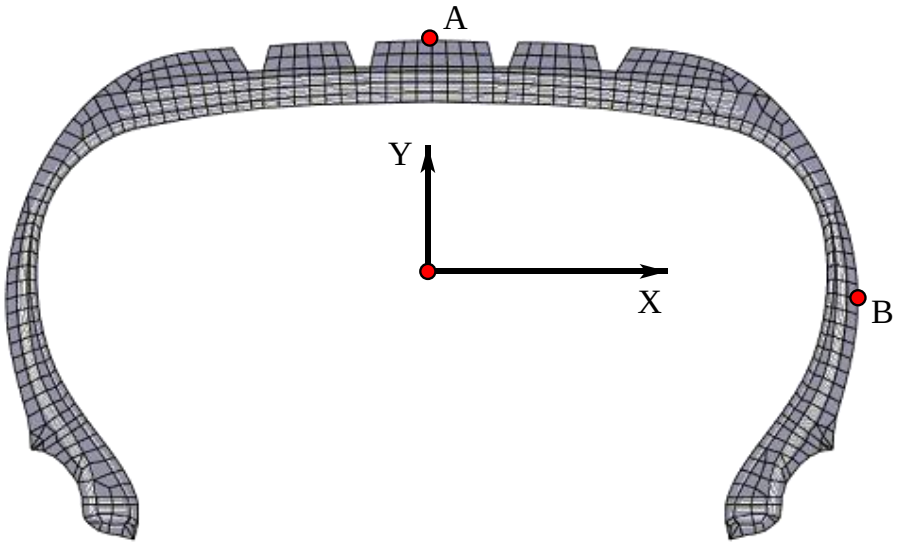

Figure 6. Tread and sidewall nodes

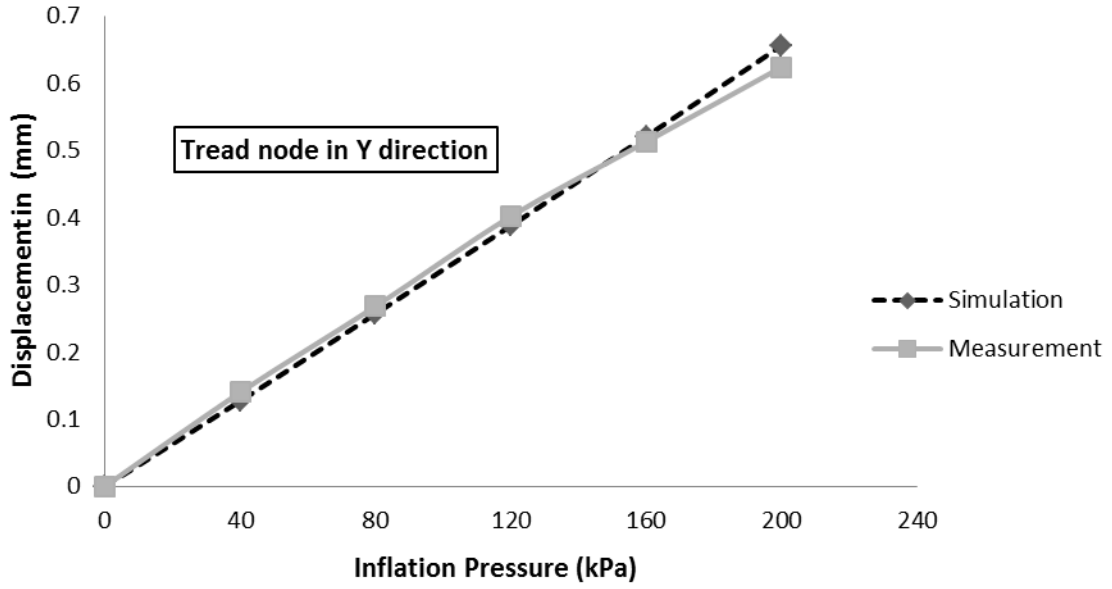

Figure 7. Displacement of tread node A in Y direction

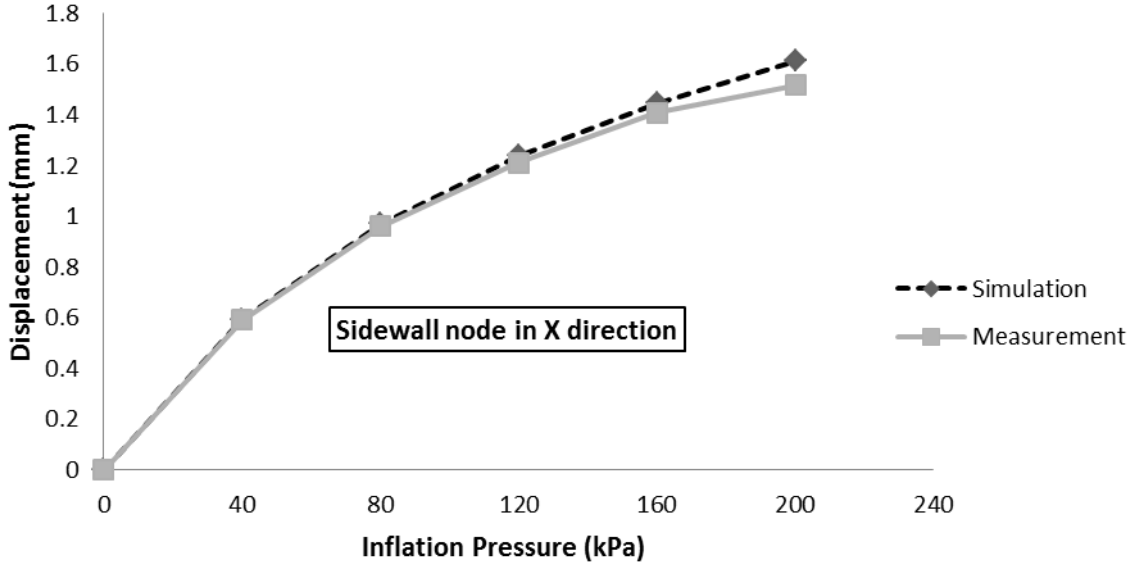

Figure 8. Displacement of the sidewall node B in X direction

2.2. Static Stiffness Analysis

2.2.1. Definition of tire/road contact

Normal contact qualification is used to restrict the movement of two contact bodies (Fig. 9). Impenetrability is used to make the constraint that the configurations V^A of body A and V^B of body B cannot penetrate into each other in the process of movement [15]. In the tire/road contact model, V^A and V^B represent the tire and road respectively.

We assume that ${}^t x_P^A$ represents the coordinate of the particle P on the surface ${}^t S^A$ of body A at time t, the distance g, between the particle and the nearest particle $Q({}^t x^B)$ on the surface ${}^t S^B$ (Fig. 9) can be expressed by:

$$ {}^t g = g({}^t x_P^A, t) = \left| {}^t x_P^A - {}^t x_Q^B \right| = \min \left| {}^t x_P^A - {}^t x^B \right| \tag{1} $$

where, ${}^t x^B$ represents the coordinate of any particle on surface ${}^t S^B$. In this study, the orientation of g, should be the same with that of ${}^t \boldsymbol{n}^B$ which represents the unit vector normal to the contact plane. Therefore, the vector ${}^t \boldsymbol{g}$ can be obtained by:

$$ {}^t\boldsymbol{g} = \boldsymbol{g}({}^t x_P^A, t) = ({}^t x_P^A - {}^t x_Q^B) \cdot {}^t \boldsymbol{n}_Q^B \quad (2) $$

In order to meet the requirement of impenetrability for the two bodies (the tire and the road), we use the following constraint to define any particle *P* on the surface ${}^t S^B$

$$ {}^t\boldsymbol{g}_n = \boldsymbol{g}({}^t x_P^A, t) = ({}^t x_P^A - {}^t x_Q^B) \cdot {}^t \boldsymbol{n}_Q^B \geq 0 \quad (3) $$

where, ${}^t\boldsymbol{g}_n > 0$ means a gap exists between the particle *P* and the surface ${}^t S^B$, while ${}^t\boldsymbol{g}_n = 0$ means the particle *P* has a contact with ${}^t S^B$. As the above function is effective for any particle on surface ${}^t S^A$ and ${}^t S^B$, the function can be described by:

$$ {}^t\boldsymbol{g}_n = \boldsymbol{g}({}^t x^A, t) = ({}^t x^A - {}^t x^B) \cdot {}^t \boldsymbol{n}^B \geq 0 \quad (4) $$

In addition, since the equivalent normal contact force is provided by the pressure, the condition of normal contact force λ_N (Fig. 9) is given by:

$$ \lambda_N \geq 0 \quad (5) $$

In the tangential direction of rolling contact analysis, Coulomb model of friction is adopted to define the tangential contact conditions. In engineering analysis, coulomb model of friction is widely used because of its characteristics of simplicity and applicability [15]. The definition in the Coulomb friction model is that slip occurs when the tangential contact force (frictional resistance) $\tau_{eq} = \sqrt{\tau_1^2 + \tau_2^2}$ equals to the critical stress $\tau_{crit} = \mu\lambda_N \geq 0$ which means that the friction force cannot be allowed to exceed the critical stress, which is:

$$ \tau_{eq} = \sqrt{\tau_1^2 + \tau_2^2} \leq \mu\lambda_N \quad (6) $$

in which μ is the coefficient of friction, τ_1 and τ_2 are shear stresses in t_1 direction and t_2 direction respectively, and λ_N represents the normal contact force. On the other hand, no relative motion between the tire and the rigid road surface occurs when $\tau_{eq} < \tau_{crit}$. In ABAQUS, the stiff viscous behavior is adopted to approximately simulate the non-relative-motion condition,

$$ \tau_\alpha = \kappa\dot{\gamma}_\alpha (\alpha = 1, 2) \quad (7) $$

in which τ_α represents the shear stress in the tangential direction, $\dot{\gamma}_\alpha$ is the tangential slip rate in the tire/road contact plane, $\kappa = \mu\lambda_N / 2\Delta\omega R$ is the stick viscosity, ω is the rotation angular velocity and *R* is the rolling radius of the tire, and Δ is the slip tolerance defined by the users. In this study, Δ was set as 0.005.

2.2.2. Vertical (radial) stiffness

2.2.2.1. Experimental tests for vertical stiffness

As a prevalent parameter for tire static analysis and validation, static stiffness has an effect on vehicle ride performance and the properties of the static stiffness is very important for tire dynamic analysis. In the program, the vertical stiffness experimental tests were carried out using the tri-axial electro-hydraulic tire dynamic rig with a 2.44 diameter drum, the configuration of which is shown in Fig. 10. The procedure of the non-rolling tire vertical stiffness test includes three steps:

1) Apply an inflation pressure to the tire. As the tests need to consider vertical stiffness at different inflation pressures, an initial inflation pressure of 200kPa is applied on the tire, which is convenient to deflate it in order that the vertical stiffness at lower inflation pressure can be obtained.

2) Move the tire into contact with the drum. In order to acquire the position of the tire when it contacts the drum with a 0 vertical load, the tire needs to be pushed toward the drum gradually, and then the position of the tire is recorded. In this step, the center of the drum, the center of the tire, and the system fixed point need to be adjusted in the same line, which is illustrated in Fig. 11.

3) Set a displacement of the tire. In this step, the position of the tire in vertical direction is determined in order to set the displacement of the tire. Different levels of displacement are applied to the tire, and the tire is pushed towards to the drum incrementally, the corresponding vertical loads are recorded by the calibrated load cell.

2.2.2.2. Static vertical stiffness simulation

The 3D tire model is obtained by revolving the 2D cross section of the tire about the rotational symmetric axis using *SYMMETRIC MODEL GENERATION, REVOLVE command. The 2D axisymmetric elements (CGAX4H and CGAX3H) were transformed into 3D solid elements (C3D8H and C3D6H). For the static contact analysis, only contact region of the tire need to be given fine meshes. The three-dimension model is composed of 50 sections, covering an angle of 320 degrees, while the rest of the model was separated into 60 sections in the tire-road contact patch region, covering an angle of 40 degrees. The objective of dividing such refined sections in contact patch region is to meet the requirements of steady state rolling analysis, and from which it should be convenient to acquire more accurate prediction of the forces and footprint (Fig. 11).

In this three-dimension model, the tire was inflated to a pressure of 200kPa, the road was defined as an analytical rigid surface, the initial contact between the tire and the road was established with a small vertical displacement in order to avoid convergence difficulties which might be influenced by the unbalanced forces. Then a vertical load of 3000N was applied on the road towards the tire rim reference node. After completing the simulation of tire deformation, the reaction force to the displacement was recorded from the rim reference node. The deformed three-dimension tire model with road surface is shown in Fig. 12.

Figure 10. Tri-axial electro-hydraulic test rig

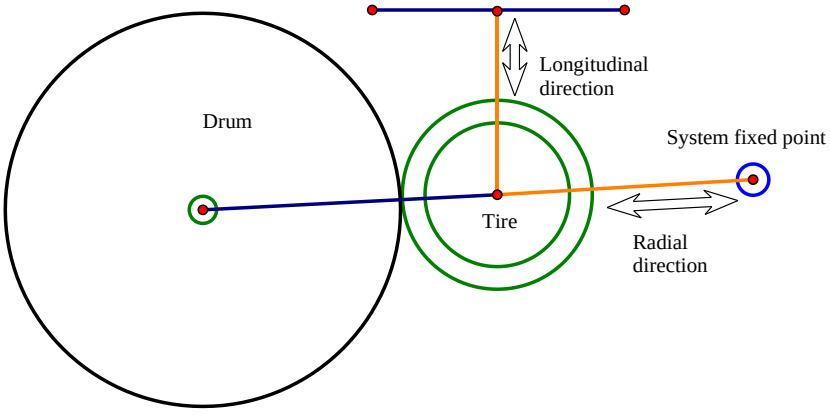

Figure 11. Schematic representation of the test rig

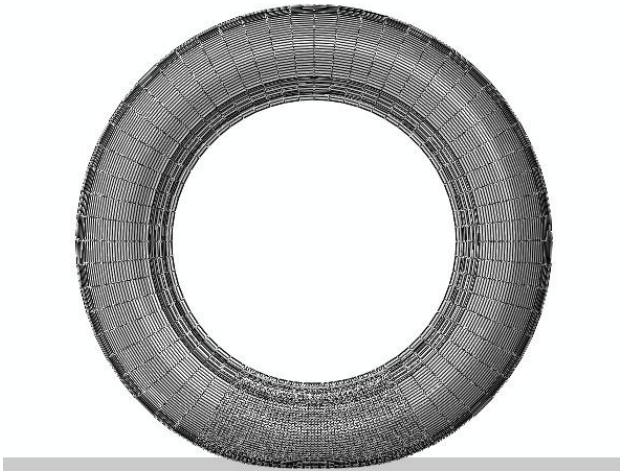

Figure 12. Deformed 3D tire model

2.3. Footprint Analysis

The size and shape of the footprint of a tire as well as the pressure distribution within the footprint are significant factors for tire properties, especially ride performance and handling properties of a vehicle. The tri-axial electro-hydraulic tire dynamic rig was also applied for footprint tests. Black ink was smeared on the tire tread, and a sheet of white paper was attached on the drum in order that the contact patch was imprinted on it, described in Fig. 13. The tire was pushed toward the drum slowly until the vertical load reached a pre-set value. In order to analyze the effect of inflation pressure and vertical load on the size and shape of the footprint, different levels of inflation pressure and vertical load were applied on the tire. The acquired footprint image was scanned into the computer and the contact area was calculated by extracting its outline and importing it to Solidworks, which are illustrated in Fig. 14.

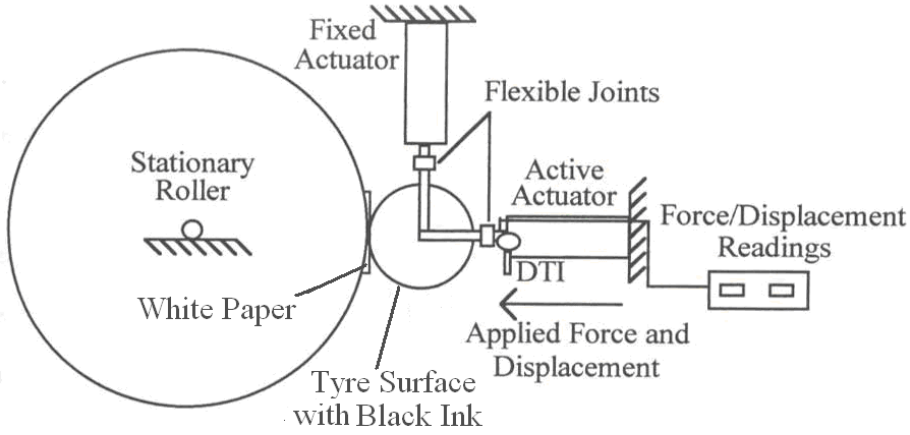

Figure 13. Configuration for footprint experiment

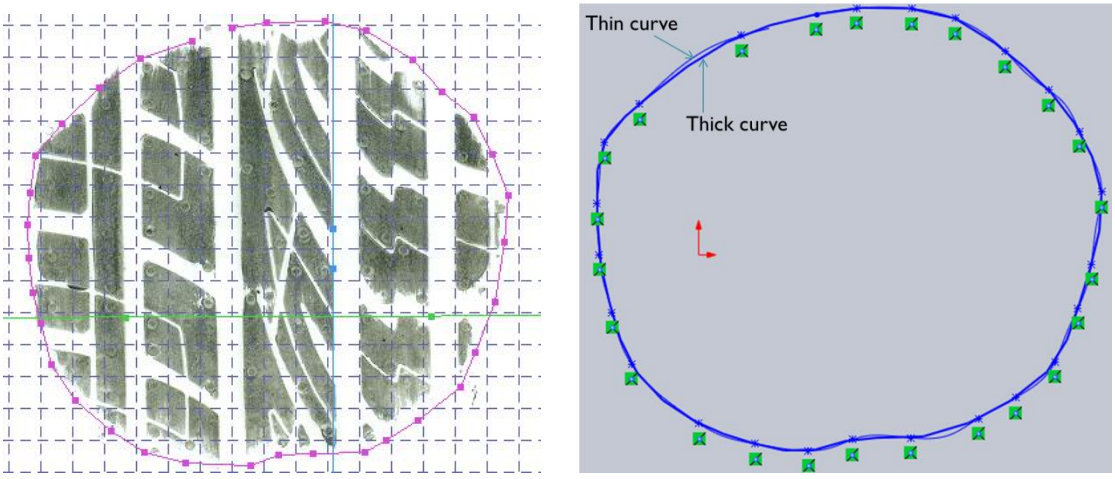

(a) (b)

Figure14. (a) Extracting the outline of footprint, (b) Contact area calculating in Solidworks (the thick one is the curve from (a) and the thin one is the fitted curve in Solidworks)

3. Results and Discussion

3.1. Comparison between the Test and Simulation Results

As the initial inflation pressure applied on the tire is 200kPa, it is convenient to carry out the static tests with lower levels of inflation pressure by deflating the tire. Different values of inflation pressure (200kPa, 160kPa, 120kPa, 80kPa, 40kPa) were applied on the tire for simulations and tests. In the tests, the vertical loads were recorded at the tire displacements of 0mm, 3mm, 6mm, 12mm and 15mm. Fig. 15 to Fig. 19 describe the comparisons of vertical stiffness between corresponding simulation and experimental tests.

From the force/displacement relationship figures shown above, it can be seen that there are approximately linear relationships between vertical loads and displacements at different inflation pressures. The vertical stiffness was obtained by fitting the relationship between vertical load and tire displacement in vertical direction using a linear curve. The com-

parison of vertical stiffness values between experimental tests and FE simulations is shown in Table 1. From Fig. 15 to Fig. 19 and Table 1, it can be seen that both of the force/displacement relationships and the vertical stiffness values at different inflation pressure conditions show satisfactory correlations between the experimental tests and FE simulations.

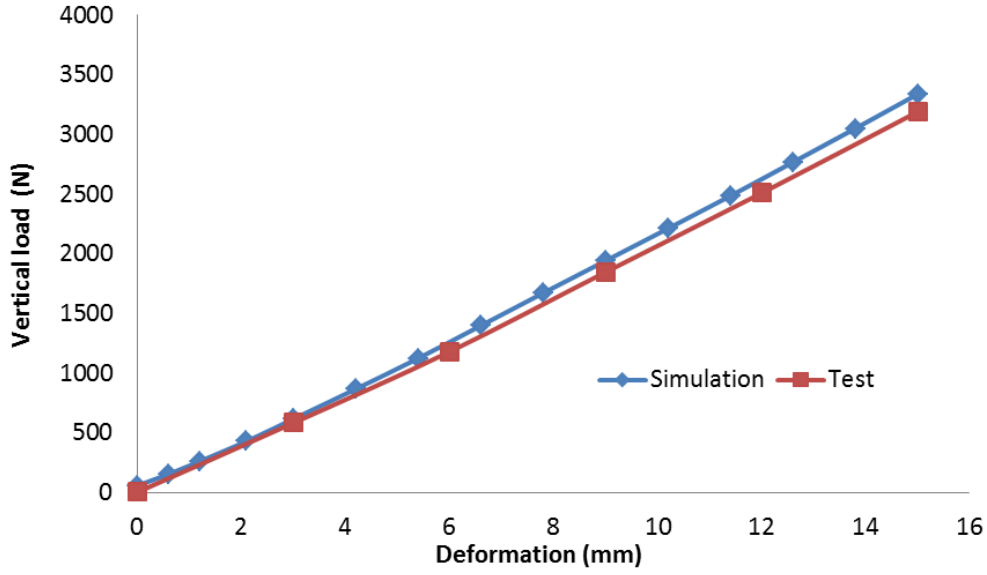

Figure 15. Force/Displacement relationships at 200kPa

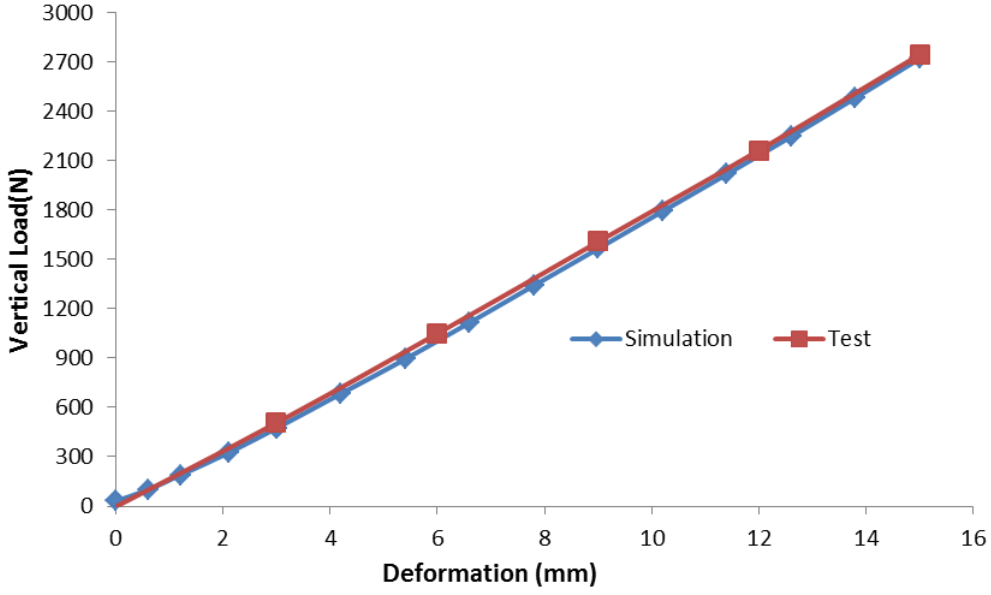

Figure 16. Force/Displacement relationships at 160kPa

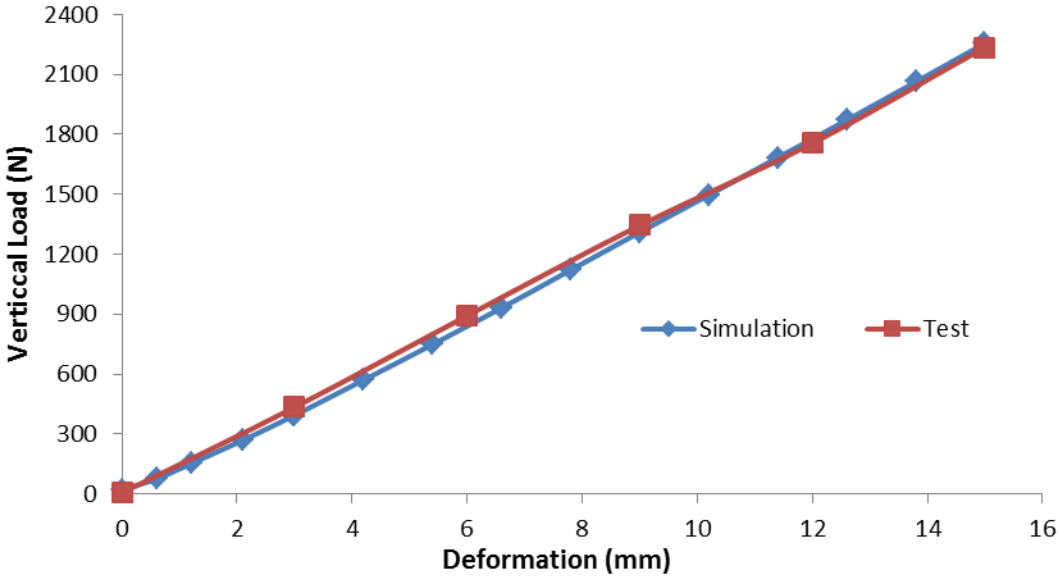

Figure 17. Force/Displacement relationships at 120kPa

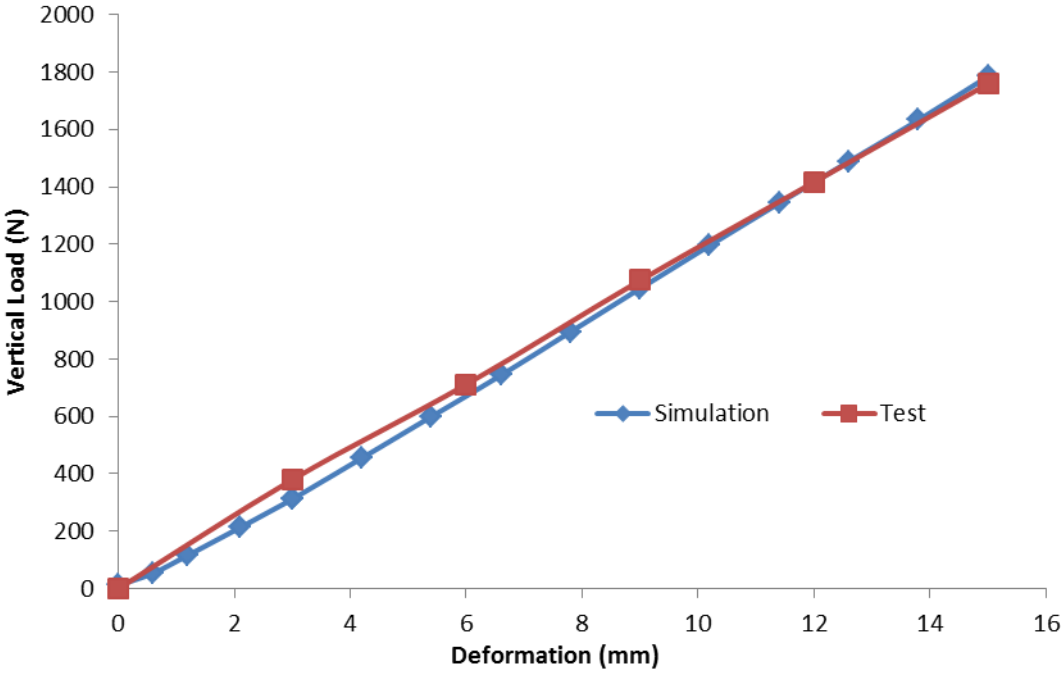

Figure 18. Force/Displacement relationships at 80kPa

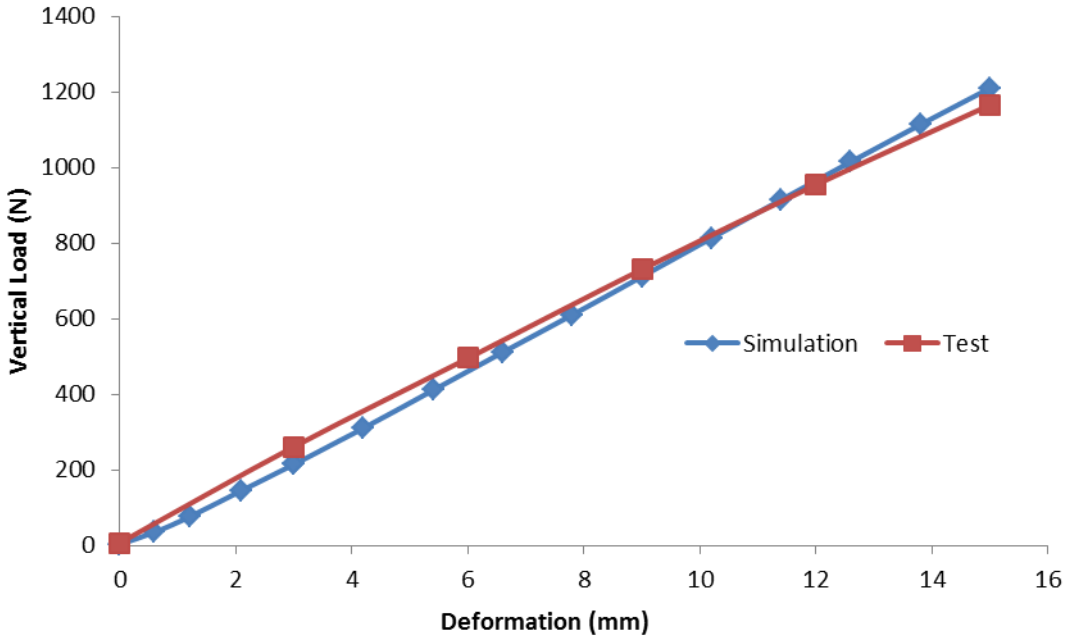

Figure 19. Force/Displacement relationships at 40kPa

Table 1. Comparison of vertical stiffness between test and simulation

Inflation pressures (kPa)	Vertical Stiffness Tests (kN/m)	Vertical Stiffness Simulation(kN/m)	Absolutely Difference (%)
200	222.53	212.83	4.36
160	180.21	178.19	1.13
120	146.31	146.8	0.33
80	118.05	119.39	1.12
40	79.55	82.23	3.26

3.2. Longitudinal Stiffness and Lateral Stiffness

Unlike vertical stiffness, the longitudinal stiffness and lateral stiffness tests are difficult to carry out because of laboratory limitations. However, with the FE program, the simulations for derivation of longitudinal and lateral stiffness can be conducted sufficiently.

In the simulation of longitudinal movement, the tire was set to contact the road with a small deflection in the vertical direction in order that an initial vertical load is obtained. The friction of the road was set as 1.0 and no slip was allowed in the simulation, and then a small displacement in the longitudinal direction was applied on the tire spindle (Fig. 20 (a)). Longitudinal stiffness can be obtained from the gradient of the relationship between longitudinal forces and longitudinal displacement of the tire center.

For the lateral stiffness simulation, a small deflection of the tire on the vertical direction towards the road was applied initially, and the same friction condition was defined in the simulation. The tire was then moved in the lateral direction up to a small displacement of 10mm, which is illustrated in Fig. 20 (b). Lateral stiffness can be obtained from the gradient of the relationship between lateral forces generated on the spindle and lateral displacement of the tire center.

In order to investigate the influence of operating conditions on longitudinal stiffness and lateral stiffness, different inflation pressures and different initial vertical deflection were applied on the tire/road contact model. Fig. 21(a) describes the relationship between longitudinal forces and longitudinal displacement of the tire with different inflation pressures, a preload in vertical direction was applied in the simulation. On the other hand, the variations of longitudinal force with different initial vertical deflections are shown in Fig. 21(b) when an inflation pressure of 200kPa was applied in the simulation. Fig. 22(a) illustrates the relationship between lateral forces variation when the tire with different inflation pressures was stretched to a displacement of 10mm, and the initial vertical deflection of the tire was set as 9mm so that the preload was applied. For different initial deflections of the tire in the vertical direction, the relationships between lateral forces and lateral displacement of the tire were illustrated in Fig. 22(b), and the inflation pressure of 200kPa was applied on the simulation.

The longitudinal stiffness can be derived by extracting the gradient of the relationship between longitudinal force and

longitudinal displacement of the tire. Table 2 shows the longitudinal stiffness values at different operating conditions, from which it can be seen that higher inflation pressure leads to higher longitudinal stiffness and higher initial vertical deflection also leads to higher longitudinal stiffness. On the other hand, lateral stiffness was also derived using the same method as longitudinal stiffness. The values of lateral stiffness at different conditions are shown in Table 2. Likewise, the lateral stiffness increases with the inflation pressure and the lateral stiffness increases when higher vertical deflection is applied in the model.

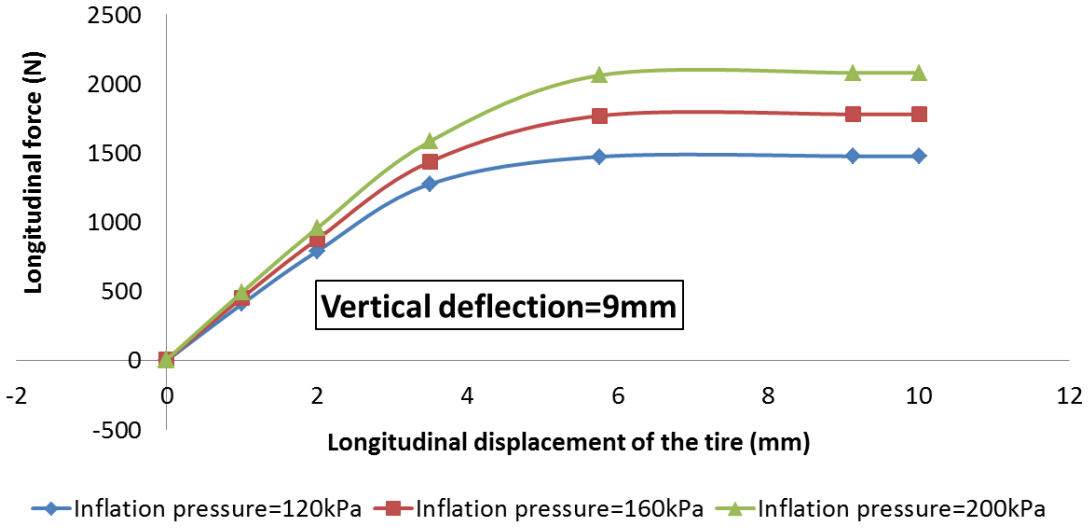

(a)

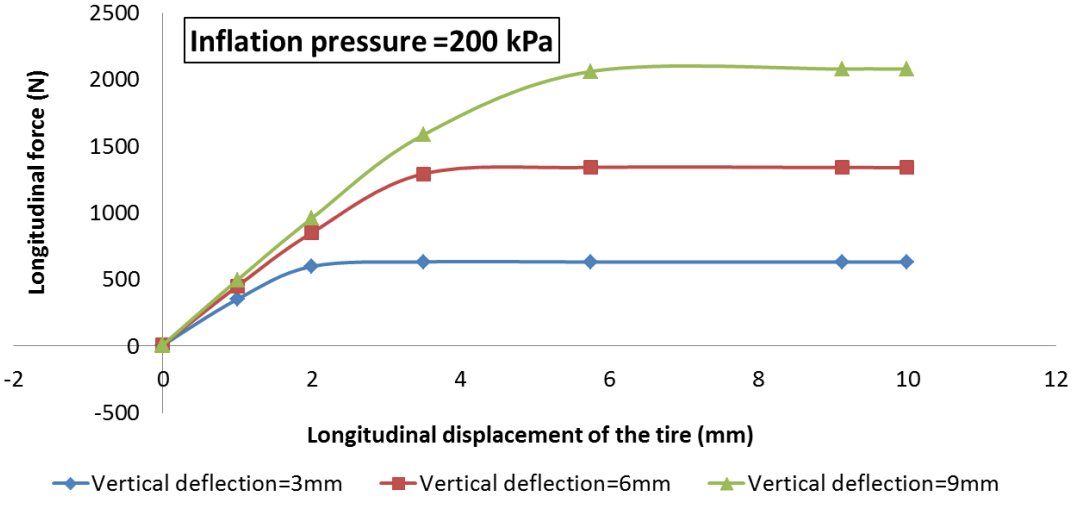

(b)

Figure 21. (a) Relationship between longitudinal forces and longitudinal displacement of the tire under different inflation pressures and (b) Relationship between longitudinal forces and longitudinal displacement of the tire with different initial vertical deflection of the tire

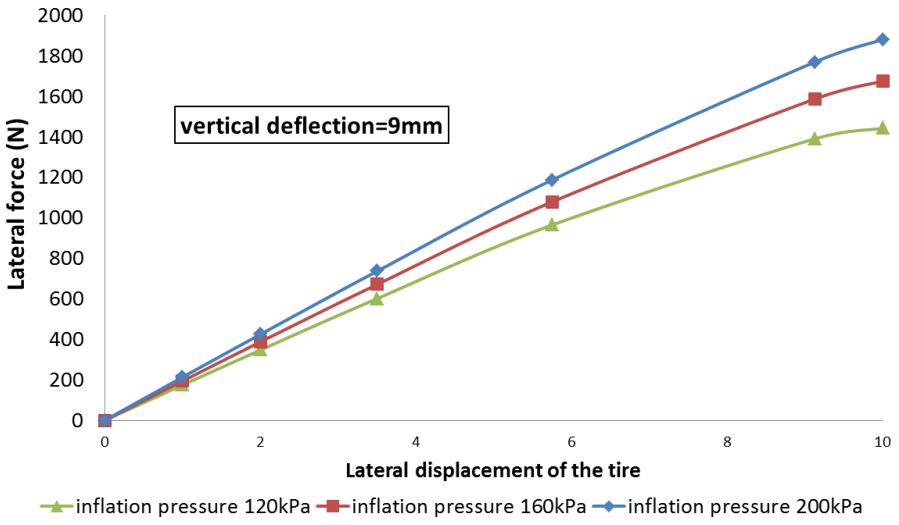

(a)

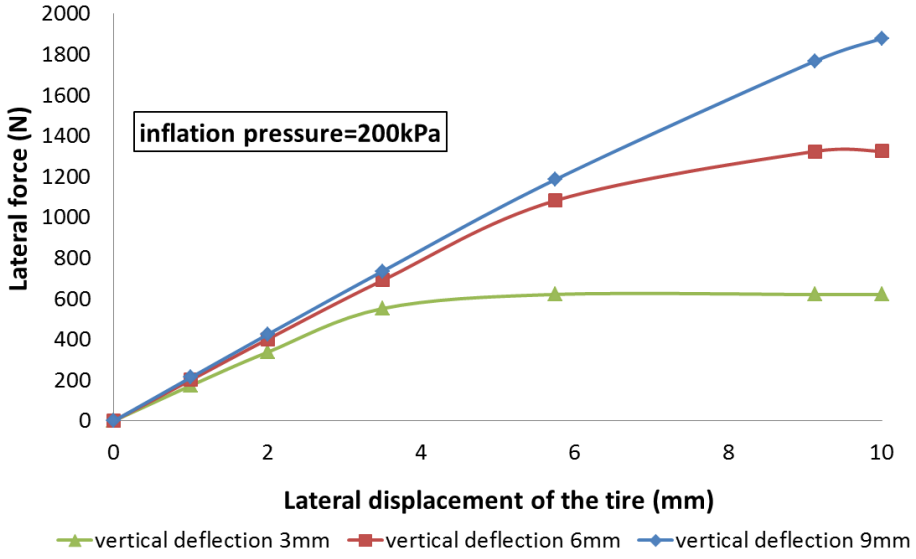

(b)

Figure 22. (a) Relationship between lateral forces and lateral displacement of the tire under different inflation pressures and (b) Relationship between lateral forces and lateral displacement of the tire with different initial vertical deflection of the tire

Table 2. Static longitudinal and lateral stiffness at different conditions

Inflation pressure	Vertical deflection 9mm	Vertical deflection 6mm	Vertical deflection 3mm
	Longitudinal stiffness (N/mm)		
120kPa	790.30	686.40	434.96
160kPa	877.39	772.20	434.96
200kPa	957.58	848.98	597.13
	Lateral stiffness (N/mm)		
120kPa	346.84	326.99	272.21
160kPa	386.87	365.12	306.78
200kPa	423.99	400.66	337.14

3.2. Footprint analysis

In the FE simulation of footprint analysis, footprint shapes and pressure distributions at different operating conditions were easily acquired by using "CAREA" and "CPRESS" in ABAQUS, in which "CAREA" described the contact area between the tire and the road, while "CPRESS" illustrated the tire/road contact pressure distribution (Fig. 23). As it is difficult to measure the pressure and force distribution in the contact region using experimental tests, it is necessary to use the tire model for the simulation. In addition, the corresponding area of footprint can also be calculated in the process of footprint analysis. In the first step of the procedure of footprint simulation, the inflation pressure was set as 200kPa, and different vertical loads of 1000N, 2000N, 3000N and 4000N were applied on the tire. In the second step, the vertical load was fixed as 3000N, and the inflation pressures of 80kPa, 120kPa, 160kPa and 200kPa were applied on the tire for footprint extraction.

As mentioned above, the area of footprint from experiment can be obtained using CAD software processing, and the FE analysis is also capable of predicting the area of tire/road contact patch. The validation of footprint areas at the operating conditions with different vertical loads is shown in Fig. 24, while Fig. 25 describes the validation of footprint areas at different inflation pressures. With the increase of vertical load, the tire has a higher deformation, which will lead to a greater contact area. On the other hand, the higher inflation pressure leads to a lower deformation, which makes the contact area smaller.

Figs. 26-28 show the footprint shapes at different vertical loads from simulations and experiments, while Figs. 29-32 describe the contact patch shapes at different operating conditions with different inflation pressures.

It can be seen that at the condition of 200kPa inflation pressure, the width of the contact patch is greater than the length of the contact patch for vertical loads of 1000N, 2000N, 3000N and 4000N. In addition, when the vertical load reaches 3000N, the contact width meets the shoulder of the tire, which is the reason that the footprint shape is not an elliptical form. For the condition with a vertical load of 3000N, when the inflation pressure is up to 80kPa, the contact length of the footprint is greater than the contact width, which is shown in Fig. 32. At a vertical load of 3000N or higher when the inflation pressure is not greater than 200kPa, the contact width reaches the shoulder of the tire which leads to a contact shape different from the elliptical form.

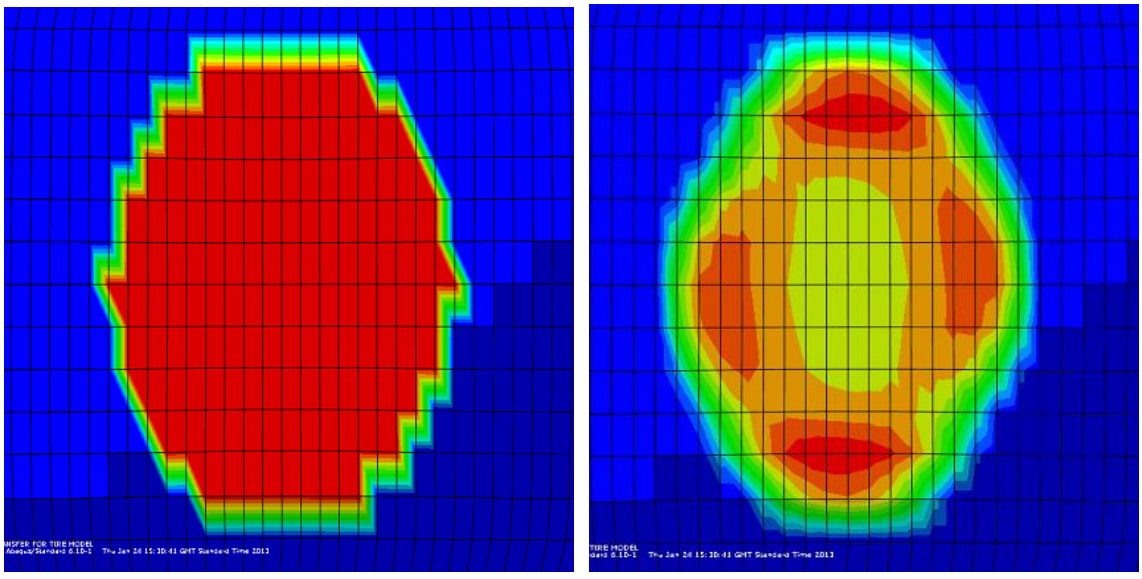

(a) (b)

Figure 23. (a) Footprint for "CAREA", (b) Footprint for "CPRESS"

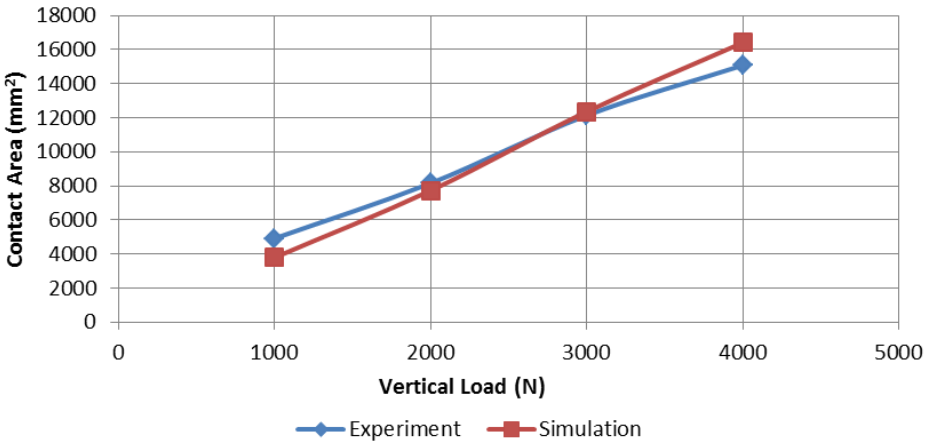

Figure 24. Footprint area at different vertical loads

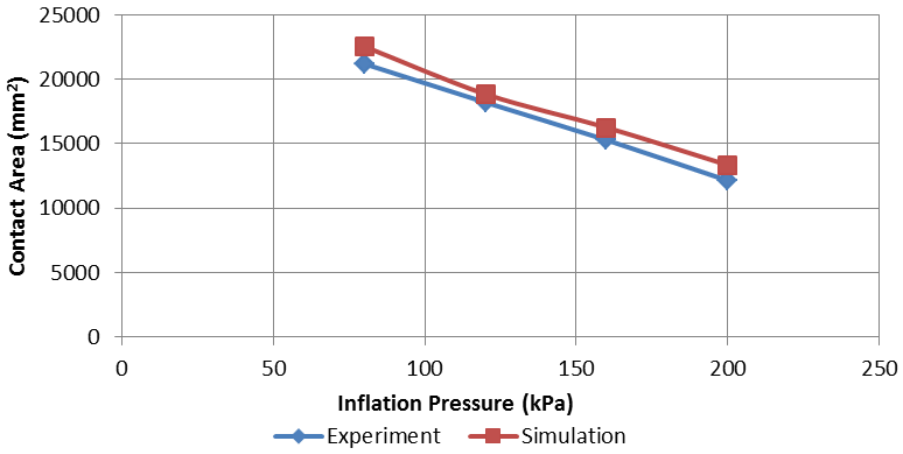

Figure 25. Footprint area at different inflation pressures

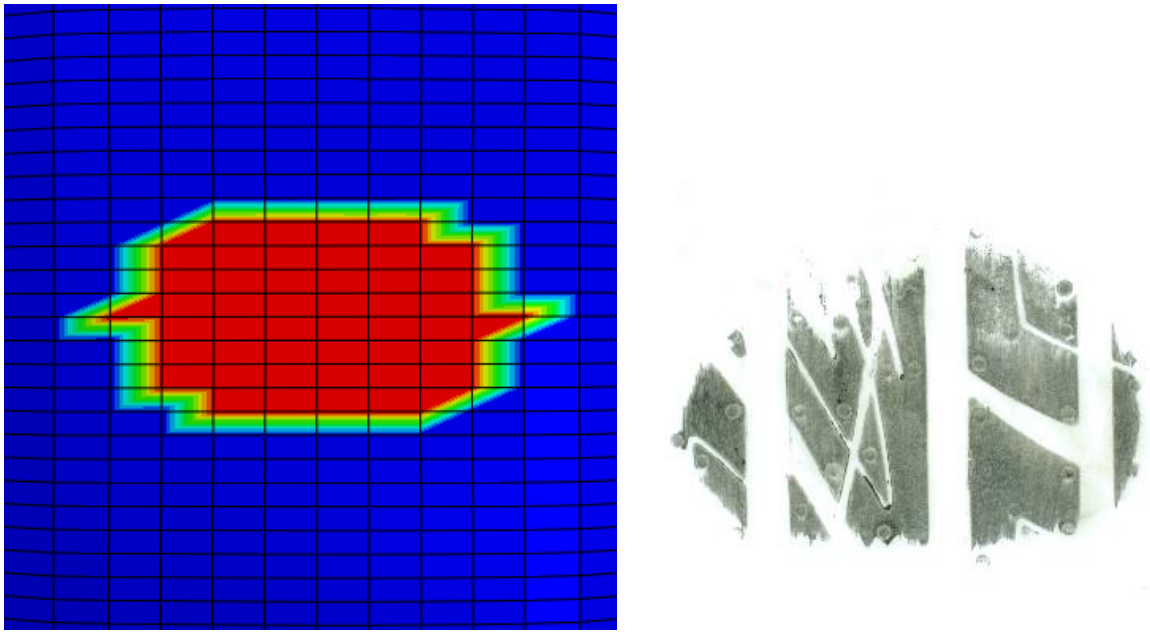

Figure 26. Footprint for 1000N vertical load, 200kPa inflation pressure

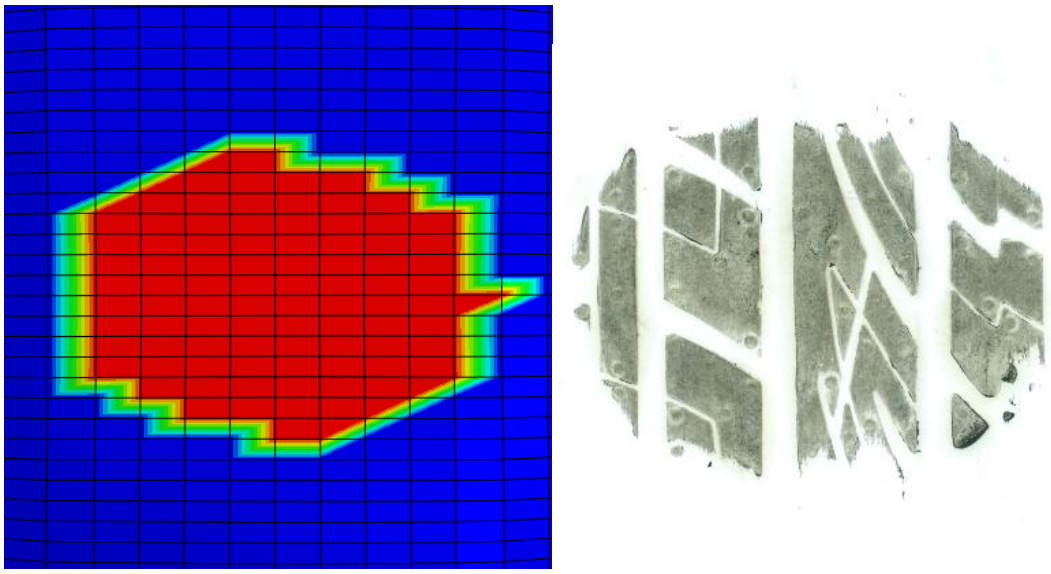

Figure 27. Footprint for 2000N vertical load, 200kPa inflation pressure

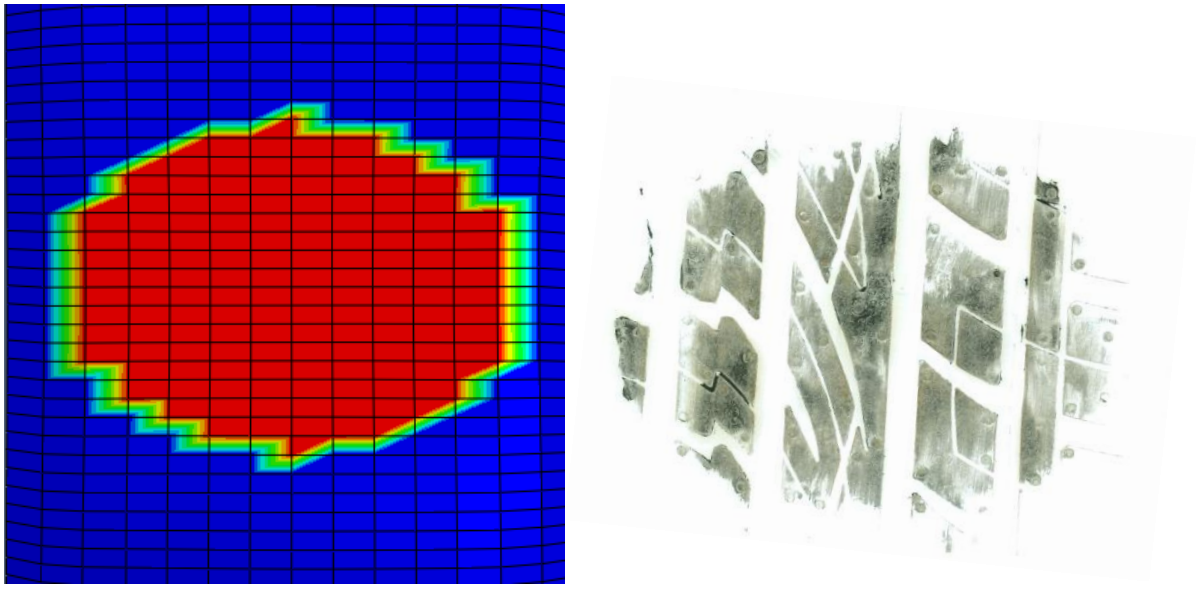

Figure 28. Footprint for 3000N vertical load, 200kPa inflation pressure

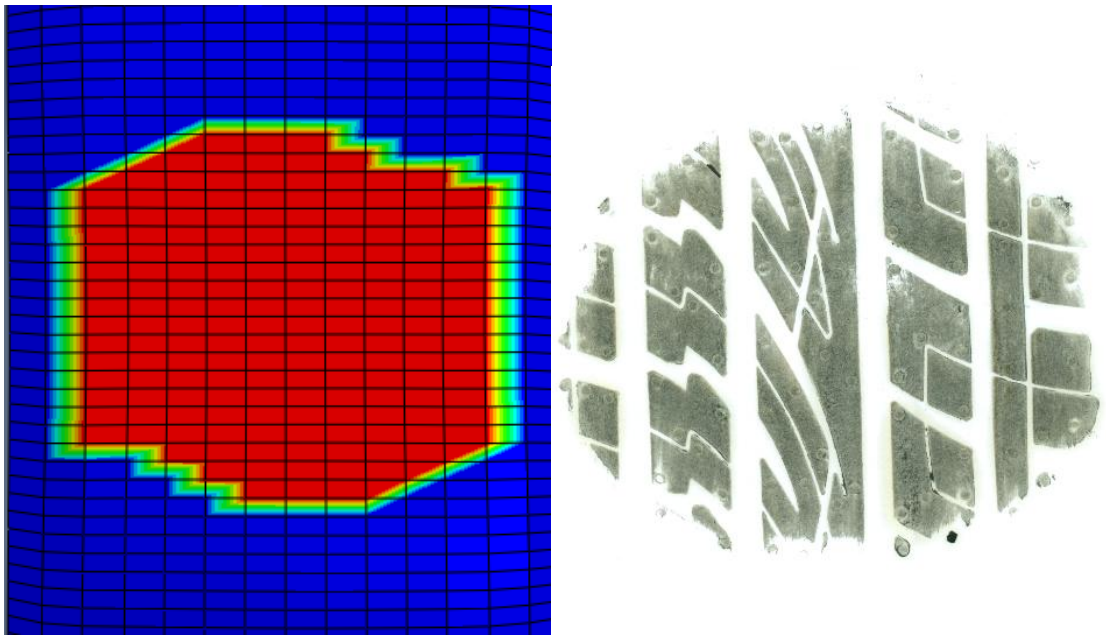

Figure 29. Footprint for 4000N vertical load, 200kPa inflation pressure

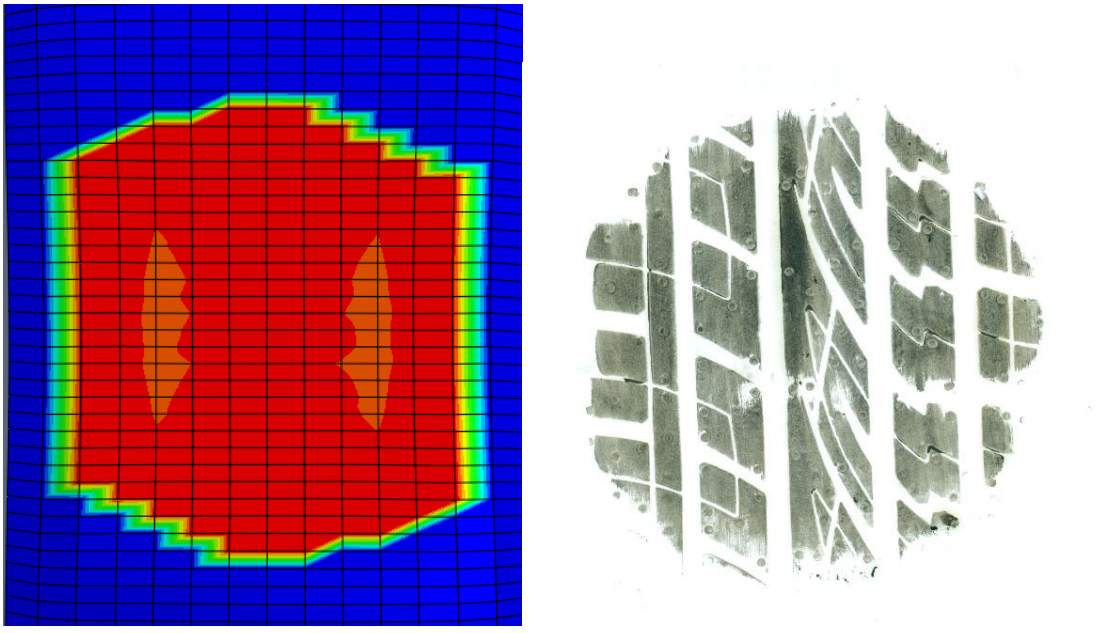

Figure 30. Footprint for 3000N vertical load, 80kPa inflation pressure

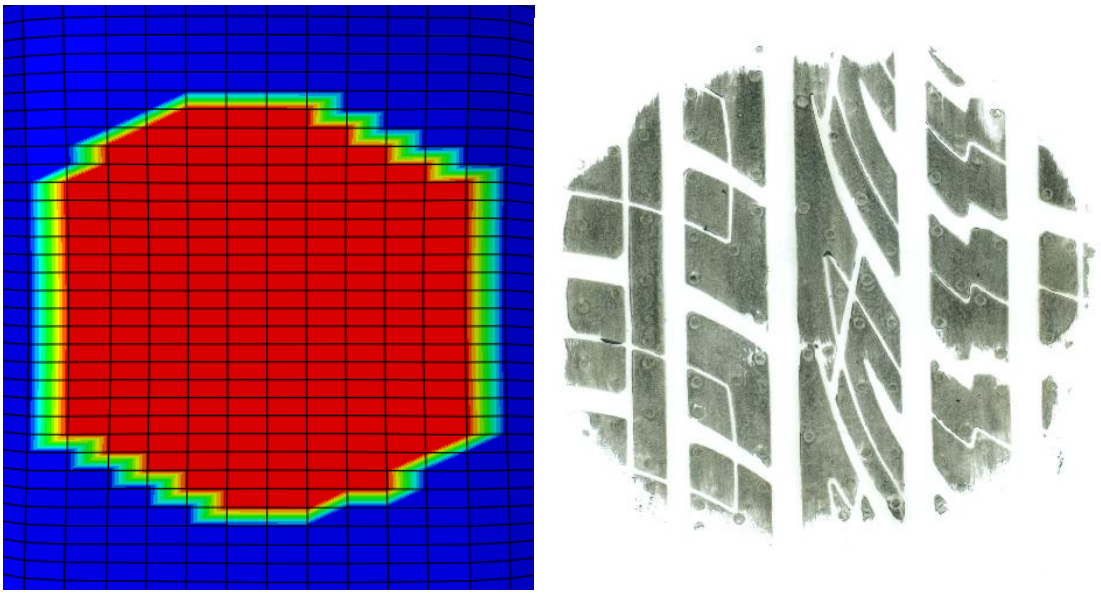

Figure 31. Footprint for 3000N vertical load, 120kPa inflation pressure

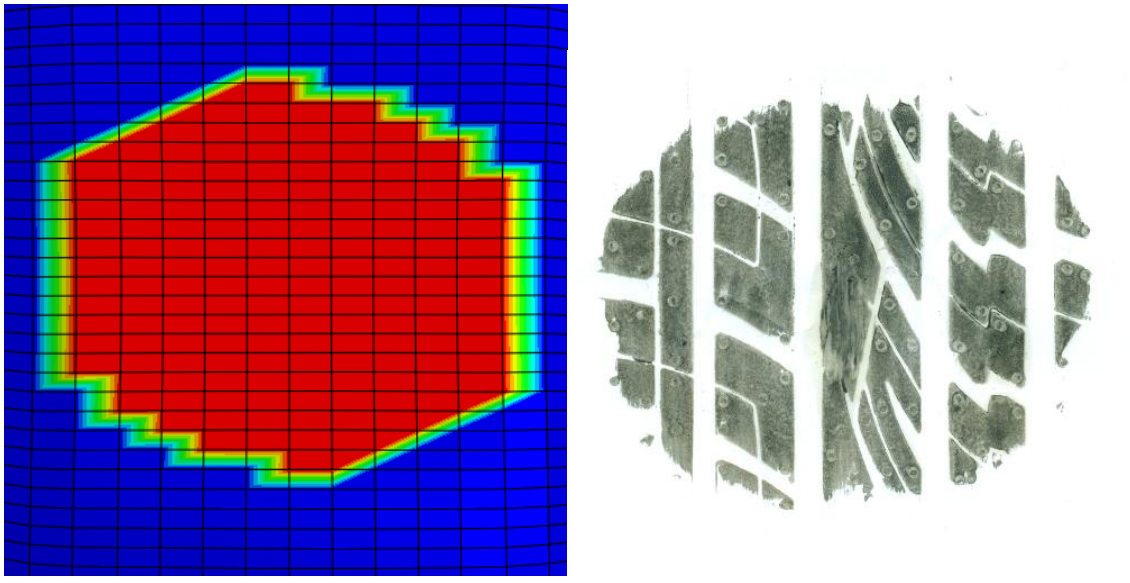

Figure 32. Footprint for 3000N vertical load, 160kPa inflation pressure

6. Conclusion

In this paper, analysis of static properties of the tire were presented. Inflation pressure analysis was conducted using 2D tire model. The 3D tire model was obtained by revolving the 2D axisymmetric tire model, and static stiffness and footprint were predicted using the 3D model. Inflation pressure analysis was presented by comparing the tire cross-section shape variation at different inflation pressures. Since it was difficult to find the variation of the cross section shapes clearly, the specified tread node and sidewall node were taken to analyze the displacements of tire tread and sidewall at different inflation pressures. In order to obtain accurate values for static stiffness and footprint, fine meshes were adopted on the contact region of the tire. Validation of vertical stiffness was carried out, and results show that the model is capable of predicting vertical stiffness at different operating conditions. The footprint areas as well as the footprint shapes at different operating conditions were validated, and satisfactory results were obtained in the comparison between simulations and experiments. Since the model is capable of prediction of static properties of the tire, it

is deemed ready for the further analyses at steady-state rolling conditions and transient dynamic conditions.

References

[1] Gipser M. FTire: a physically based application-oriented tyre model for use with detailed MBS and finite-element suspension models. Vehicle System Dynamics 2005; 43(1):76-91.

[2] Tielking J.T. Plane Vibration Characteristics of a Pneumatic Tire Model. SAE Transactions 1966; 74: 126

[3] Keltie R.F. Analytical Model of the Truck Tire Vibration Sound Mechanism. Journal of the Acoustical Society of America 1982;71(2): 359-367

[4] Qiu X.D., Liu J., Men Y.X. A Modified Point-Contact Tire Model for the Simulation of Vehicle Ride Quality. Journal of Terramechanics, 1993; 30(3): 133-141.

[5] Kao B.G. A Three-Dimensional Dynamic Tire Model for Vehicle Dynamic Simulations. Tire Science and Technology 2000; 28(2): 72-95.

[6] Kao B.G. Tire Vibration Modes and Tire Stiffness. Tire Science and Technology 2002; 30(3):136-155.

[7] Shim T., Margolis D. An analytical tyre model for vehicle simulation in normal driving conditions. International Journal of Vehicle Design 2004; 35(3): 224-240.

[8] Dihua G., Jin S., Yam L.H. Establishment of model for tire steady state cornering properties using experimental modal parameters. Vehicle System Dynamics 2000; 34(1): 43-56.

[9] Shang J., Guan D.H., Yam L.H. Study on tire dynamic cornering properties using experimental modal parameters. Vehicle System Dynamics 2002; 37(2):129-144.

[10] Guo K., Ren L. A Unified Semi-Empirical Tire Model with Higher Accuracy and Less Parameters. 1999, SAE International.

[11] Brinkmeier M., Nackenhorst U., Petersen S., Von Estorff O. A finite element approach for the simulation of tire rolling noise. Journal of Sound and Vibration 2008; 309(1): 20-39.

[12] Yang X., Olatunbosun O. A., Bolarinwa E.O. Materials testing for finite element tire model. SAE International Journal of Materials & Manufacturing 2010; 3(1), 211-220.

[13] Tönük E., Ünlüsoy Y.S. Prediction of automobile tire cornering force characteristics by finite element modeling and analysis. Computers & Structures 2001; 79(13): 1219-1232.

[14] Xia, K. Finite element modeling of tire/terrain interaction: Application to predicting soil compaction and tire mobility. Journal of Terramechanics 2011; 48(2): 113-123.

[15] Wang X. Finite Element Method. 2003, Beijing, China: Tsinghua University Press.